Synchrotron 3D microtomography of halite aggregates during experimental pressure solution creep and evolution of the permeability

François Renard
Laboratoire de Géophysique Interne et Tectonophysique, Université Joseph Fourier, Grenoble, France
Physics of Geological Processes, University of Oslo, Oslo, Norway

Dominique Bernard
Institut de Chimie de la Matière Condensée de Bordeaux, Pessac, France

Xavier Thibault and Elodie Boller
European Synchrotron Radiation Facility, Grenoble, France

Received 29 January 2004; revised 27 February 2004; accepted 10 March 2004; published 3 April 2004.

[1] Pressure solution creep is one of the possible processes of mechano-chemical deformation that controls porosity and permeability variations in the upper crust. The three-dimensional geometry of the porous network of halite aggregates was imaged during compaction driven by pressure solution creep using X-ray synchrotron computed microtomography. This technique can be used to monitor individual grain contacts and whole aggregate textural changes during deformation. By reconstructing sub-volumes, the 3D porosity of the aggregates was extracted. The time-resolved decrease in permeability during porosity reduction was calculated by solving the Stokes equations. The permeability remained isotropic and decreased from 2.1 to 0.15 Darcy after 18.2% compaction. Two microscopic mechanisms can explain the permeability reduction: grain indentation and pore connectivity reduction by precipitation on the free surface of pore throats. *INDEX TERMS:* 3902 Mineral Physics: Creep and deformation; 3947 Mineral Physics: Surfaces and interfaces; 5114 Physical Properties of Rocks: Permeability and porosity; 5139 Physical Properties of Rocks: Transport properties; 5194 Physical Properties of Rocks: Instruments and techniques. **Citation:** Renard, F., D. Bernard, X. Thibault, and E. Boller (2004), Synchrotron 3D microtomography of halite aggregates during experimental pressure solution creep and evolution of the permeability, *Geophys. Res. Lett.*, *31*, L07607, doi:10.1029/2004GL019605.

1. Introduction

[2] The deformation of rocks by dissolution-transport-precipitation mechanisms (i.e., pressure solution) is considered to be an important ductile deformation mechanism during diagenesis of sedimentary rocks [*Heald*, 1955; *Weyl*, 1959] and compaction of fault gouges during the seismic cycle [*Gratier et al.*, 2003]. This deformation mechanism is responsible for time-dependent porosity and permeability variations over geological times.

[3] The driving force for pressure solution in an aggregate is related to stress variations along the grain surface [*Paterson*, 1973]. Pressure solution occurs as a response to a non-zero effective stress, i.e., the normal stress component σ_n across a grain contact is greater than the stress on the free pore surface of the same grain. Thus, the chemical potential can be seen to vary along the surface of a grain, driving a diffusive flux of solutes from the contact area to the free pore surface. The high stress at grain contacts causes dissolution of the minerals at the grain boundary, transport of the dissolved matter in a fluid phase out of the grain boundary and precipitation of this material in the pore space on the less stressed faces of the grains [*Weyl*, 1959; *Rutter*, 1976].

[4] As inelastic deformation occurs, the permeability of a rock varies. *Popp et al.* [2001] have shown that microcracks dynamics controls the permeability evolution during triaxial deformation of dry rock salts samples. When water is present, rock salt can creep and deform in the pressure solution regime [*Rutter*, 1976; *Spiers and Brzesowsky*, 1993]. In this case, the micromechanisms for permeability variations are no more driven by brittle fracturing but by dissolution-precipitation processes that may strongly modify the geometry of the pores.

[5] The aim of this study is twofold: 1) quantify how the porosity and the permeability of salt aggregates vary with deformation, 2) characterize the micromechanisms of permeability reduction. For these purposes, 3D X-ray microtomography (μCT) was successfully applied for visualizing several halite aggregate samples and for monitoring the time-dependent compaction. This technique provides 3D data that allow estimating the transport properties of the samples [*Lindquist et al.*, 2001; *Mees et al.*, 2003].

2. Time-Resolved Pressure Solution Creep

2.1. Experimental Set-Up

[6] A series of creep experiments was performed on halite (pure sodium chloride) aggregates (Table 1). This rock salt material represents a "generic" analogue of a sedimentary rock that has been widely used because high enough pressure solution creep rates can be measured in a reasonable laboratory time scale [*Hickman and Evans*, 1991; *Spiers and Brzesowsky*, 1993; *Schutjens and Spiers*, 1998; *Martin et al.*, 1999; *Renard et al.*, 2001; *Dysthe et al.*, 2002]. The principle of the compaction technique in specially designed oedemetric (uniaxial) cells has been described by *Renard et al.* [2001, Figure 1]. The salt was

0094-8276/04/2004GL019605$05.00

Table 1. Halite Aggregates Characteristics

Sample	Resolution	Stress	Duration
A	4.91 μm	0.13 MPa	3 days
B	4.91 μm	0.13 MPa	3 days
F	0.7 μm	0.63 MPa	7 days

sieved and the 100–150 μm fraction was kept. The aggregate in its saturated solution was poured into a hollow Plexiglas cylinder. The solution is first de-aerated using a vacuum pump in order to avoid the formation of gas bubbles during the experiment. The load was then applied and the cell sealed with silicone oil to prevent water evaporation. The normal stress was transmitted through a spring with a constant load of 1.3 or 6.3 bars depending on the experiment, the temperature was around 20°C and the fluid pressure of the saturated solution was atmospheric. The fluid was drained vertically and expelled from the aggregate during compaction.

2.2. X-ray Synchrotron Computed Microtomography

[7] Several series of radiographs were acquired on beam line ID19 at the European Synchrotron Radiation Facility. For each series, 1500 radiographs were taken with a Frelon 2K camera developed by the ESRF detector group (2048 × 2048 pixels, 12 bits) while rotating the sample through 180°. The μCT technique allows the 3D X-ray adsorption property of the sample to be reconstructed inverting the Radon transform using a back projection algorithm. As the halite and pore water have different absorption values, they can be differentiated in the reconstructed volumes. With the optics chosen, the pixel sizes are 4.91 μm (sample diameter 10.05 mm) and 0.7 μm (sample diameter 1.3 mm). Respective resolutions were better than 9 μm and 2 μm. The energy was 25 and 35 keV for 0.7 μm and 4.91 μm spatial resolutions respectively. The main advantage of this technique is that it is not destructive and the same sample can be measured during deformation (see reviews on this subject by *Mees et al.* [2003]).

[8] A first scan was performed before any stress was imposed on the aggregate to obtain the initial state. Scans were then performed periodically (scan duration 1 to 2 hours), every 12 hours for 3 days (4.91 μm resolution) and every 24 hours for 7 days (0.7 μm resolution). During the scan, the stress on the sample was released to avoid any deformation during data acquisition. These stress free periods were corrected on the compaction curves. Once the radiographs had been acquired, the stack of slices of the tested volume was reconstructed. The gray dynamics of the pictures was reduced to the [0 255] range, for data storage capacity reasons. The result was a set of volume data on which pore space and grain geometry can be quantified during each deformation step (Figure 1).

3. Results

3.1. Compaction Creep and Pore Network Evolution

[9] The vertical shortening of the cylindrical sample was measured directly on the radiographs. The compaction was checked to ensure its overall homogeneity in the sample. The height, $x(t)$ was estimated from the radiographs resulting in a measurement of the uniaxial strain $\varepsilon(t) = (x_0 - x)/x_0$ where x_0 stands for the initial height of the sample. The samples were compacted by up to 18% in three days (Figure 2a). The strain rate decreased from 2.10^{-6} s^{-1} initially to 3.5 10^{-7} s^{-1} at 18% compaction.

[10] To verify that pressure solution is the main deformation mechanism, the same grains were monitored before and during deformation. No microcracking of the grains was resolved above 0.7 μm resolution. A sub-volume of sample F corresponding to the same two grains at the start of deformation and after 11% vertical shortening is shown on Figure 3. Initially, the two grains were not in contact, and after 7 days of compaction, one grain has indented the other by relative displacement. The fluid-grain boundary can be extracted (Figure 3b) and it is shown that contact healing may have occurred because the final grain boundary has a thickness below the spatial resolution of the μCT technique (0.7 μm).

[11] Salt that dissolved at the grain contacts precipitated on the free surface where the normal stress is lower. When precipitation occurred in a narrow pore, it can close this pore throat. Therefore the pore connectivity can decrease significantly, even if the grains were not indented (Figure 4).

3.2. Permeability Calculations

[12] With the volumetric data obtained, it was possible to separate the solid phase from the pore fluid as these two

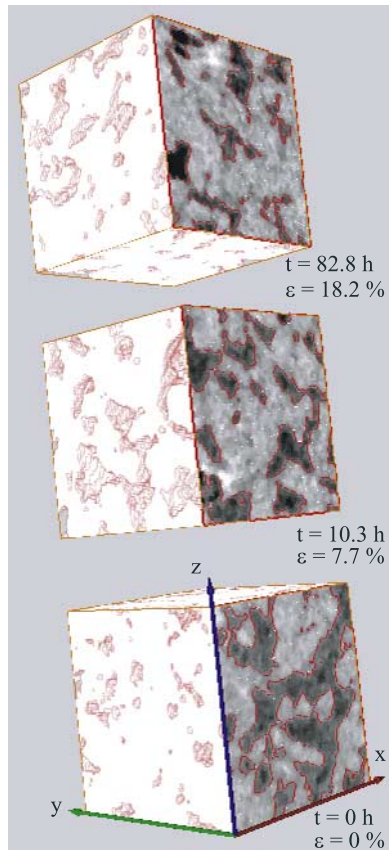

Figure 1. 100 × 100 × 100 pixel subvolume (4.91 μm resolution, 491^3 μm^3) extracted from sample B at initial stage (bottom), after 10.3 hours (middle) and after 82.8 hours (top). These data, showing the reduction in porosity with deformation (ε), are used for permeability calculations (salt in light grey, pores in dark, grain-pore interface in red).

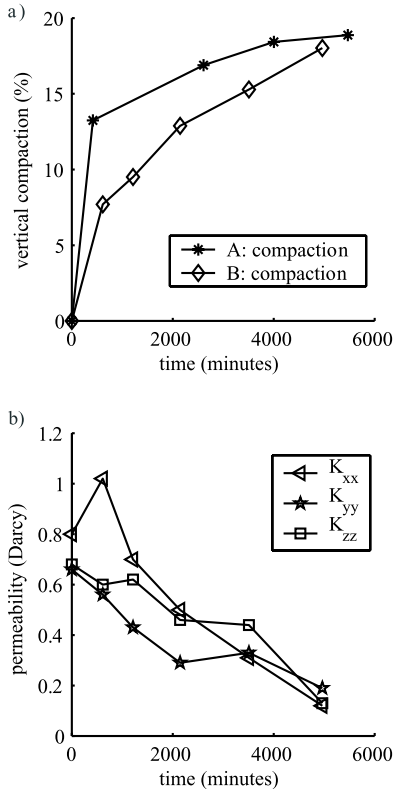

Figure 2. a) Compaction curves for samples A and B. b) Calculated permeability variation in sample B. K_{xx}, K_{yy}, and K_{zz} correspond to the three principle components of the permeability tensor.

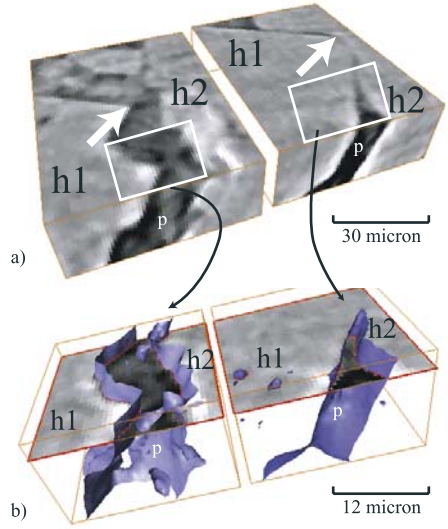

Figure 3. a) Two grains of halite before (left, initial aggregate) and after (right, 11% deformation) indentation by pressure solution in sample F. The arrows indicate the indentation of grain h1 into grain h2. The pore space (p) appears darker. b) Extraction of the pore surface on two sub-volumes showing that the grain contact has disappeared and contact healing has occurred.

phases had different X-ray absorption properties. The same absorption threshold, calibrated using the porosity of the initial sample, was chosen for all the samples at different amount of compaction. The geometry of the pore space was used to calculate the permeability tensor.

[13] Using the volume averaging method it can be demonstrated that the tensorial generalized form of Darcy's law is the macroscopic equation describing the flow through a porous medium of a fluid obeying Stokes equations at the local scale [*Sahimi*, 1995; *Whitaker*, 1999]. This method also provides a partial differential problem, the closure problem, giving a tool to compute the permeability tensor directly from the local geometry. The form of this problem demonstrates that permeability is an implicit function only of the local geometry.

[14] Even when a 3D geometrical characterization of the local geometry is available, through μCT for instance, a numerical solution of the closure problem is computationally demanding and very sensitive to the quality of the 3D information. Nevertheless, the change of scale approach is the only real alternative to semi-empirical approaches based on simplified local geometry (like the capillary tubes used for the Kozeny-Carman formula).

[15] The closure problem is a dimensionless generalized Stokes problem expressing the effects of the macroscopic pressure gradient on the local velocity perturbation. This problem was solved for 3D binarized volumes extracted at different amounts of compaction (Figure 1). The solution is a 3D tensor field which gives the complete permeability tensor averaging [*Anguy et al.*, 1994; *Bernard*, 1995; *Whitaker*, 1999].

[16] In this first series of computations, the time-dependent change in a unique sub-volume was considered. The trend highlighted corresponds to what could be expected. A more generalized study taking into account the complete

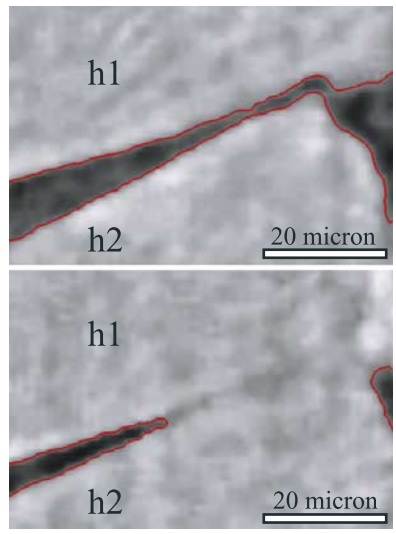

Figure 4. Two grains of halite (h1 and h2) before (top) and after (bottom) pressure solution in sample F. The pore throat between the two grains has closed by precipitation on the free surface, without any relative displacement or indentation between the two grains.

volume will be necessary to verify precisely that the sub-volume (Figure 1) is indeed representative of the whole sample and that the permeability tensor calculation does not depend significantly on the choice of this sub-volume.

[17] The symmetry of the tensor is not a condition used for the calculation. It has been verified *a posteriori* that the tensor was nearly symmetric, as it should be. A typical calculated permeability tensor is given below, for sample B after 15.2% vertical shortening; where the total porosity was 14.5% and the connected porosity was 13.9%. The porosity variations are similar to that measured through the compaction curves.

$$\begin{bmatrix} \mathbf{K_{xx}} & \mathbf{K_{xy}} & \mathbf{K_{xz}} \\ \mathbf{K_{yx}} & \mathbf{K_{yy}} & \mathbf{K_{yz}} \\ \mathbf{K_{zx}} & \mathbf{K_{zy}} & \mathbf{K_{zz}} \end{bmatrix} = \begin{bmatrix} 0.305 & 0.028 & 0.100 \\ 0.028 & 0.327 & -0.021 \\ 0.099 & -0.022 & 0.438 \end{bmatrix} \text{Darcy}$$

On sample B for which the volumetric data were the least noisy, the mean permeability decreased by a factor 14 as deformation increased from 0 to 18.2% (Figure 2b). The tensor remained isotropic even if the compaction was vertically oriented. Note that small permeability anisotropy of the sample could not be detected by our calculations as it can be hidden in the numerical noise.

4. Discussion and Conclusion

[18] During deformation by pressure solution, grain shapes were modified as salt dissolved at grain contacts and precipitated on the free surfaces. The total surface area of the contacts increased, thus reducing the normal stress and the rate of deformation; this is why the strain rate decreased with time (Figure 2a). An additional effect was the healing of the grain contacts that slowed down compaction, as proposed by *Hickman and Evans* [1991].

[19] The permeability evolution has been calculated on the same sample during deformation and was shown to decrease as compaction occurs (Figure 2b). Two mechanisms at the grain scale can explain the permeability reduction. On one hand, grain indentations reduced the pore volume (Figure 3), on the other hand, precipitation can close pore throats (Figure 4) and therefore strongly modify fluid channels and pore connections. Unfortunately, the experimental set-up used did not allow measuring the permeability directly on the samples.

[20] The underlying principle of this study was to use the high spatial resolution offered by synchrotron radiation to perform X-ray tomography during pressure solution. The main advantage is that this non-destructive method enables the deformation of individual grains and even grain interfaces to be monitored over the entire sample. The main results are as follows:

[21] Grain contacts have been imaged and it has been observed that grain boundary thickness was less than the resolution of the μCT technique (0.7 μm), indicating that contact healing may have occurred.

[22] 3D μCT data of the porous skeleton were acquired and these were used to calculate the time-resolved variation in the permeability tensor during deformation. The permeability remained isotropic during uniaxial compaction. At the grain scale, the mechanisms responsible for permeability decrease were identified.

[23] **Acknowledgments.** The project has been supported by the CNRS (Action Thématique Innovante and INSU Mi-Lourds). It is part of projects SI-849 and ME-580 at ESRF. We would like to thank R. Candela, C. Pequegnat and D. Tisserand for their technical help.

References

Anguy, Y., D. Bernard, and R. Ehrlich (1994), The local change of scale method for modeling flow in natural porous media (I): Numerical tools, *Adv. Water Resour.*, *17*, 337–351.

Bernard, D. (1995), Using the volume averaging technique to perform the first change of scale for natural random porous media, in *Advanced Methods for Groundwater Pollution Control*, edited by G. Gambolati and G. Verri, pp. 9–24, Springer-Verlag, New York.

Dysthe, D. K., Y. Podladchikov, F. Renard, J. Feder, and B. Jamtveit (2002), Universal scaling in transient creep, *Phys. Rev. Lett.*, *89*, 246,102.

Gratier, J.-P., P. Favreau, and F. Renard (2003), Modelling fluid transfer along Californian faults when integrating pressure solution crack-sealing and compaction processes, *J. Geophys. Res.*, *108*(B2), 2104, doi:10.1029/2001JB000380.

Heald, M. T. (1955), Stylolites in sandstones, *Geology. J.*, *63*, 101–114.

Hickman, S. H., and B. Evans (1991), Experimental pressure solution in halite—The effect of grain interphase boundary structure, *J. Geol. Soc. London*, *148*, 549–560.

Lindquist, B. W., A. Venkatarangan, J. Dunsmuir, and T.-F. Wong (2001), Pore and throat size distributions measured from synchrotron X-ray tomographic images of Fontainebleau sandstones, *J. Geophys. Res.*, *105*, 21,509–21,527.

Martin, B., K. Roller, and B. Stoeckhert (1999), Low-stress pressure solution experiments on halite single-crystals, *Tectonophysics*, *308*, 299–310.

Mees, F., R. Swennen, M. Van Geet, and P. Jacobs (2003), Applications of X-ray Computed Tomography in the Geosciences, *Geol. Soc. Spec. Publ.*, *215*.

Paterson, M. S. (1973), Nonhydrostatic thermodynamics and its geologic applications, *Rev. Geophys.*, *11*, 355–389.

Popp, T., H. Kern, and O. Schulze (2001), Evolution of dilatancy and permeability in rock salt during hydrostatic compaction and triaxial deformation, *J. Geophys. Res.*, *106*, 4061–4078.

Renard, F., D. Dysthe, J. Feder, K. Bjørlykke, and B. Jamtveit (2001), Enhanced pressure solution creep rates induced by clay particles: Experimental evidence in salt aggregates, *Geophys. Res. Lett.*, *28*, 1295–1298.

Rutter, E. H. (1976), The kinetics of rock deformation by pressure solution, *Philos. Trans. R. Soc. London*, *283*, 203–219.

Sahimi, M. (1995), *Flows in Porous Media and Fractured Rock: From Classical Models to Modern Approaches*, John Wiley, Hoboken, N. J.

Schutjens, P. M. T., and C. J. Spiers (1998), Intergranular pressure solution in NaCl: Grain-to-grain contact experiments under optical microscope, *Oil Gas Technol.*, *54*, 729–750.

Spiers, C., and R. Brzesowsky (1993), Densification behavior of wet granular salt: Theory versus experiment, paper presented at the Seventh Symposium of Salt, Elsevier, Amsterdam, v. I, 83–92.

Weyl, P. K. (1959), Pressure solution and the force of crystallization—A phenomenological theory, *J. Geophys. Res.*, *69*, 2001–2005.

Whitaker, S. (1999), *The Method of Volume Averaging*, Kluwer Acad., Norwell, Mass.

D. Bernard, Institut de Chimie de la Matière Condensée de Bordeaux 87, Av. du Dr. Albert Schweitzer, F-33608 Pessac, France.

E. Boller and X. Thibault, European Synchrotron Radiation Facility, BP 220, F-38043 Grenoble cedex, France.

F. Renard, LGIT, BP 53, F-38041 Grenoble, France. (francois.renard@obs.ujf-grenoble.fr)